JACS
JOURNAL OF THE AMERICAN CHEMICAL SOCIETY

Article

pubs.acs.org/JACS

Twisted Hemithioindigo Photoswitches: Solvent Polarity Determines the Type of Light-Induced Rotations

Sandra Wiedbrauk,[†,§] Benjamin Maerz,[‡,§] Elena Samoylova,[‡] Anne Reiner,[‡] Florian Trommer,[‡] Peter Mayer,[†] Wolfgang Zinth,[‡] and Henry Dube*[,†]

[†]Department für Chemie, Ludwig-Maximilians-Universität München, D-81377 Munich, Germany

[‡]Institut für Biomolekulare Optik, Ludwig-Maximilians-Universität München, D-80538 Munich, Germany

Supporting Information

ABSTRACT: Controlling the internal motions of molecules by outside stimuli is a decisive task for the generation of responsive and complex molecular behavior and functionality. Light-induced structural changes of photoswitches are of special high interest due to the ease of signal application and high repeatability. Typically photoswitches use one reaction coordinate in their switching process and change between two more or less-defined states. Here we report on new twisted hemithioindigo photoswitches enabling two different reaction coordinates to be used for the switching process. Depending on the polarity of the solvent, either complete single bond (in DMSO) or double bond (in cyclohexane) rotation can be induced by visible light. This mutually independent switching establishes an unprecedented two-dimensional control of intramolecular rotations in this class of photoswitches. The mechanistic explanation involves formation of highly polar twisted intramolecular charge-transfer species in the excited state and is based on a large body of experimental quantifications, most notably ultrafast spectroscopy and quantum yield measurements in solvents of different polarity. The concept of pre-twisting in the ground state to open new, independent reaction coordinates in the excited state should be transferable to other photoswitching systems.

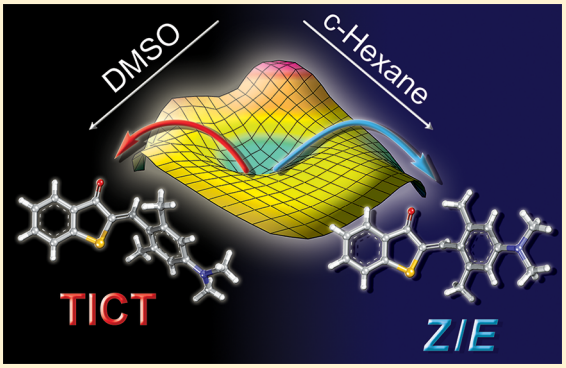

INTRODUCTION

The control of molecular motions is a decisive task in the construction of functional molecules[1] and molecular machines.[2,3] Such control can only be achieved if the equilibrating force of the Brownian motion is counteracted by input of external energy. Whether that energy is dissipated randomly or via a specific motion depends on the chemical setup and the degrees of freedom of the particular molecule. The highest precision for controlled molecular motion has been achieved with synthetic molecular motors,[4,5] the most efficient of which undergo unidirectional rotation around a double bond, using the energy of light as power source.[6−8] Light is arguably the most effective energy input, and therefore photoswitches—molecules that react reversibly to light in a specific way—are frequently employed as "engine" units to trigger specific motions[9−11] and/or events in functional molecular[12−21] or biological[22−27] systems. Understanding the mechanisms of light-induced photoswitching and the specific electronic and geometric changes during that process[28,29] is thus of fundamental importance for our ability to consciously design complex molecular behavior.

We have recently described unexpected electronic substitution effects on the photoisomerization rates of hemithioindigo (HTI) dyes—an emerging class of photoswitches[30]—and explained them mechanistically.[31] The deexcitation and photoreaction of those HTI derivatives proceeds along the double-bond isomerization coordinate,[29] despite the presence of another single bond, which could in principle undergo light-induced rotation as well (Figure 1). In the present Article we describe new HTI derivatives that can

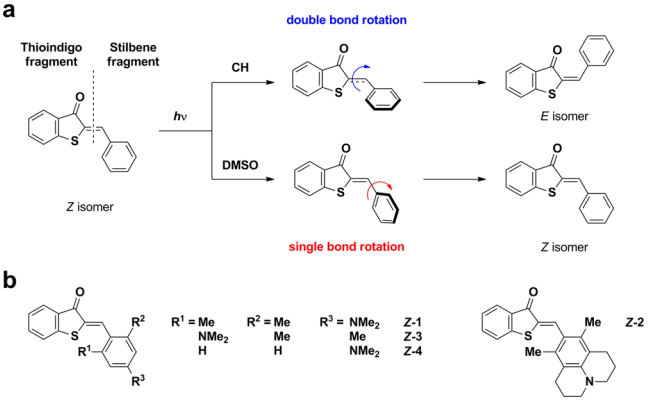

Figure 1. (a) Possible light-induced motions in HTI photoswitches. Depending on the conditions, double or single bond rotations could take place. (b) HTI derivatives *Z*-**1** to *Z*-**4** to test selective light-induced bond rotations.

Received: June 22, 2016
Published: August 29, 2016

DOI: 10.1021/jacs.6b05981
J. Am. Chem. Soc. 2016, 138, 12219−12227

undergo both types of rotations during de-excitation. The right choice of solvent makes it possible to selectively follow either pathway, which represents an exquisite control over more complex light-induced molecular motions in this class of photoswitches.

HTIs consist of a central double bond, which connects a thioindigo fragment with a stilbene fragment via one additional single bond (Figure 1). During the de-excitation of unsubstituted HTI, a double-bond rotation takes place, with additional pyramidalization of the corresponding carbon atoms.[29] A mechanism that involves hula-twisting[32−35]—i.e., simultaneous rotation around the double and single bonds—is typically not considered to take place during photoisomerization of this class of molecules. However, because of the presence of a rotatable C−C single bond, there is another possible de-excitation mechanism, which involves rotation of that single bond instead of the double bond. For HTIs with planar geometry, bearing substituents with moderate electronic effects, such de-excitation pathways have not been described so far, as their behavior can be explained satisfactorily by exclusive double-bond rotation.[36,37] However, in related stilbenes with strong donor−acceptor substitution, twisted intramolecular charge-transfer (TICT)[38,39] species, which are formed by motions along a single-bond rotation coordinate,[40−45] have frequently been discussed.[46,47] Similar behavior has also been described for substituted styrenes.[48] Recently, arylamine-substituted stilbenes have been found to de-excite exclusively via the formation of TICT species in polar solvents but undergo efficient double-bond isomerization in nonpolar solvents.[49−51]

EXPERIMENTAL SECTION

HTIs *Z*-**1** to *Z*-**4** were synthesized following established protocols for HTI synthesis,[52−54] as outlined in the Supporting Information. Their full characterization and details about time-resolved and quantum yield measurements are also described therein.

RESULTS AND DISCUSSION

Twisted HTIs. In order to test TICT states in HTI photoswitches, we prepared new HTIs *Z*-**1** to *Z*-**3**, which possess substituents in both *ortho*-positions of the stilbene fragment (Figure 1b). The already described planar HTI *Z*-**4** was used as a control compound, which is not expected to undergo TICT formation in the excited state.[31]

Each of these four HTIs bears one strong electron-donating dialkylamino substituent; the electronic effects of the additional alkyl substituents in *Z*-**1** to *Z*-**3** remain very small in comparison. Two-fold *ortho*-substitution in *Z*-**1** to *Z*-**3** leads to a significant twist along the single-bond axis, as can be seen from the corresponding crystal structural data (see Figure 2a for representations of the molecular structures). The dihedral angle around the rotatable single bond is largest for HTI *Z*-**1** (75°), followed by the corresponding angle in HTIs *Z*-**2** (60°) and *Z*-**3** (32°). In contrast, HTI *Z*-**4** has a planar geometry, with an angle of only 7° in the crystal structure. A similar twisting of HTIs *Z*-**1** to *Z*-**3** is also present in solution, which could directly be proven by chemical shift analysis of indicative proton signals in the ^{1}H NMR spectra (Figure 2b,c and Figure S14). Especially the signal of proton **a** (in the *ortho*-position of the sulfur atom) provided clear evidence for planarity in HTI *Z*-**4** and the out-of-plane twisting of the stilbene fragment in HTIs *Z*-**1** to *Z*-**3**. Depending on its twist angle, the magnetic ring current of the stilbene fragment leads to sizable upfield (if the ring is twisted as in HTIs *Z*-**1** to *Z*-**3**) or downfield shifts (if the ring is in plane with the thioindigo fragment as in HTI *Z*-**4**) of the proton **a** signal (Figure 2c). The unbiased chemical shift of proton **a** was obtained from the corresponding *E* isomeric HTIs, which place the stilbene fragment far away from proton **a**. Indeed, a similar chemical shift for this proton was found for all *E* isomeric HTIs, independent of their specific substitution. In Figure 2b, the NMR spectra of the *Z* and *E* isomers of HTI **1** are compared exemplarily to illustrate the ring current effects on proton **a** in the *Z* isomers. Thus, both solution NMR and crystal structure analysis show that the *ortho*-substitutions lead to a considerable twisting around the C−C single bond.

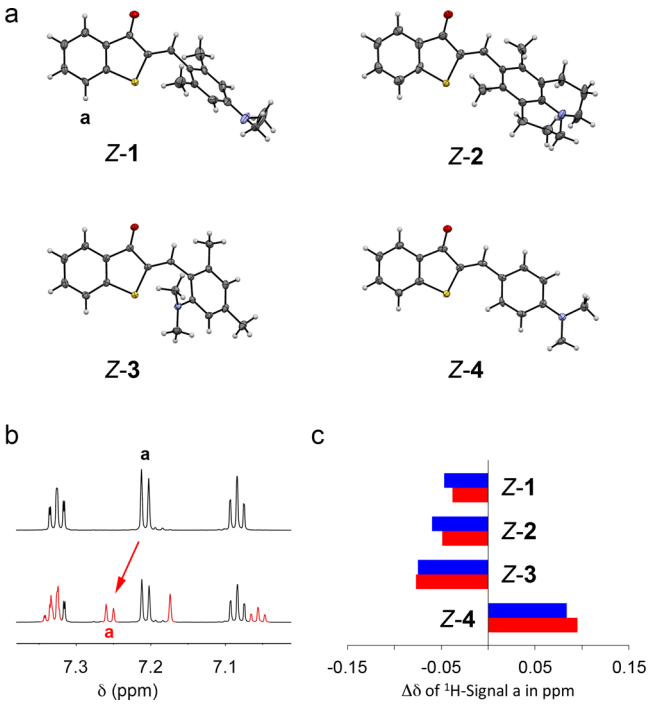

Figure 2. HTIs *Z*-**1** to *Z*-**4** used in the present study and their preferred conformations. (a) Molecular structures obtained from crystal structure analysis. (b) Aromatic region of the 800 MHz ^{1}H NMR spectra of HTI *Z*-**1** in cyclohexane (CH)-d_{12} before (top) and after (bottom) partial *Z*/*E* photoisomerization. The indicative shift of the NMR signal of proton **a** upon *Z*/*E* isomerization is emphasized by the red arrow. (c) Chemical shift differences of proton **a** ($\Delta\delta = \delta_Z - \delta_E$) upon *Z*/*E* isomerization of HTIs **1**−**4** in CH (blue bars) and CH_2Cl_2 (red bars).

Stationary Absorption and Fluorescence. In Figure 3, the stationary absorption and fluorescence spectra of HTIs *Z*-**1** to *Z*-**4** are compared in solvents of different polarity. The planar HTI *Z*-**4** shows a moderate solvatochromism of absorption and fluorescence. The solvatochromism of the fluorescence is stronger, showing that the molecule is less polar in the Franck−Condon (FC) region than in the S_1 minimum (S_{1Min}) from which the fluorescence occurs.

The absorption spectra of twisted HTIs *Z*-**1** to *Z*-**3** are somewhat broader but are only moderately affected by the polarity of the solvent. Similar to planar HTI *Z*-**4**, the FC region of twisted HTI *Z*-**1** is not significantly more polar than the ground state S_0. The stationary fluorescence of HTIs *Z*-**1** and *Z*-**2** is very different from the fluorescence of HTI *Z*-**4**. A very strong solvatochromism is seen in polar solvents, leading to Stokes shifts of more than 200 nm. In very polar solvents such as DMF, DMSO, or acetonitrile (see Figure 3 and Figures

DOI: 10.1021/jacs.6b05981
J. Am. Chem. Soc. 2016, 138, 12219−12227

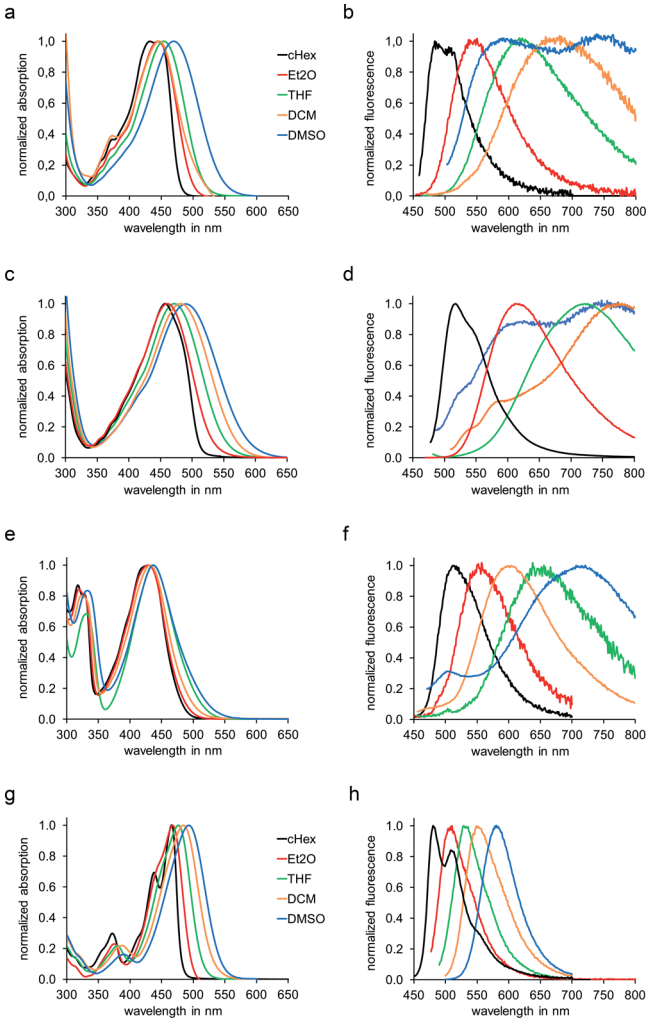

Figure 3. Normalized stationary absorption (left) and fluorescence (right) spectra of *Z*-**1** (a,b), *Z*-**2** (c,d), *Z*-**3** (e,f), and *Z*-**4** (g,h). The different solvents are color-coded: CH, black; Et_2O, red; THF, green; CH_2Cl_2, orange; and DMSO, blue. Strong solvatochromism and dual fluorescence are seen for *Z*-**1** and *Z*-**2**.

S32 and S34), indications for dual fluorescence are clearly observed. However, the very broad single-maximum fluorescence seen in solvents of intermediate polarity (CH_2Cl_2, THF, EtOAc, acetone) also suggests an underlying secondary fluorescence component.

The stationary spectra of HTI *Z*-**3** (see Figure 3 and Figures S35 and S36) show a behavior similar to those of HTIs *Z*-**1** and *Z*-**2**, i.e., very strong solvatochromism of the fluorescence leading to large Stokes shifts in polar solvents. For HTI *Z*-**3** there is no clear evidence for dual fluorescence in any of the solvents used, but the severe broadening of the single-maximum fluorescence bands and their shapes point to a second fluorescing species.

Time-Resolved Absorption of the *Z* Isomers. The ultrafast kinetics taking place after photoexcitation were followed by transient absorption spectroscopy with a 150 fs resolution in solvents of different polarity at 22 °C. The most important kinetic data are summarized in Table 1. A more comprehensive compilation of all time constants is given in Tables S5–S8. An overview of the transient absorption data is given in Figure 4a–f, where the absorption changes are plotted versus probing wavelength and delay time for HTIs *Z*-**1**, *Z*-**2**, and *Z*-**4**. More detailed information on the reaction dynamics is obtained from the analysis of the absorption transients by a rate equation model. The corresponding fit with exponential functions supplies decay times of the transient states and spectra of the fit amplitudes. These decay-associated spectra (DAS) are given in Figure 4g,h. As in our previous study of HTI *Z*-**4** in CH_2Cl_2,[31] these analyses revealed several time constants for the absorption dynamics in each case, which are assigned and discussed in detail in the Supporting Information. In the following we focus on the most important time constants to describe the excited-state dynamics, i.e., the decay of the initially populated minimum on the S_1 hyperpotential surface S_{1Min} (τ_{SE}), the *Z*/*E* photoisomerization ($\tau_{Z/E}$), and the decay of a new and very polar state (τ_T).

For the reference compound HTI *Z*-**4**, very fast nuclear motions and solvent reorganization are observed directly after excitation to the FC point before the structure reaches the excited-state minimum S_{1Min}. The relaxed excited state S_{1Min} is well recognized in all solvents by small red-shifted ground-state bleaches (GSB) and stimulated emissions (SE) where the red-shift increases with solvent polarity. The decay of this excited electronic state is connected with *Z*/*E* photoisomerization. Its rate $k_{Z/E} = 1/\tau_{Z/E}$ is solvent dependent and decreases for HTI *Z*-**4** moderately with increasing polarity of the solvent. In cyclohexane (CH), the fastest rate $k_{Z/E}$ is observed with a lifetime $\tau_{Z/E}$ = 4.8 ps, and in DMSO, the slowest rate is found with a lifetime $\tau_{Z/E}$ = 41 ps. This slowing down of *Z*/*E* photoisomerization with increasing solvent polarity indicates that a significantly polar S_{1Min} state is involved.

For twisted HTI *Z*-**1**, one observes the same initial absorption changes as for HTI *Z*-**4** in nonpolar CH (Figure 4a). The decay of the excited-state features and the appearance of the *E* isomer absorption are more rapid than for HTI *Z*-**4**, with $\tau_{Z/E}$ = 1.8 ps. Another striking feature is the stronger absorption changes at late delay times, which point to a more efficient formation of the *E* isomer. Indeed, the direct determination of the photochemical quantum yield $\phi_{Z/E}$ leads to a value of $\phi_{Z/E}$ = 56% (see below). Apparently the steric interactions imposed by the *ortho*-substitutions guide HTI *Z*-**1** efficiently toward isomerization in the nonpolar solvent.

When HTI *Z*-**1** is dissolved in more polar solvents, the transient absorption dynamics deviate strongly from those of the planar reference compound *Z*-**4**. These deviations are evident for HTI *Z*-**1** in CH_2Cl_2 (see Figure 4b,h). Even at first glance the 2D display (Figure 4b) shows a completely new pattern. Global fitting of the time-resolved absorption data in CH_2Cl_2 revealed five components; the corresponding DAS are plotted in Figure 4h. The time-resolved experiments clearly show that a new intermediate state occurs in twisted HTI *Z*-**1** in medium-polar CH_2Cl_2. This state is an excited electronic state with red-shifted SE and new excited-state absorption (ESA) features. The characteristic patterns of this state are always found for photoexcited *Z*-**1** in polar solvents. The time constant for formation of this long-lasting state is connected to the decay of the S_{1Min}, and the amplitudes depend on the specific solvent as well as the specific decay time. For the planar reference compound HTI *Z*-**4** we do not see any indication for such a state, independent of solvent polarity. Since this state occurs only in the twisted molecules, we denote it T and its decay time τ_T. The spectral features related to the excited state T show a strong red-shift of the long-wavelength ESA and SE with increasing solvent polarity. These observations indicate that the excited state T is significantly stabilized by the high

DOI: 10.1021/jacs.6b05981
J. Am. Chem. Soc. 2016, 138, 12219–12227

Table 1. Kinetic Data of the De-excitation and Quantum Yields of the *Z*/*E* Photoisomerization ($\phi_{Z/E}$) as well as Fluorescence (ϕ_{fl}) of HTIs *Z*-1 to *Z*-4

solvent	solvent polarity, $E_T(30)$/kcal mol^{-1}	$\phi_{Z/E}$/%	ϕ_{fl}/%	τ_{SE}/ps	$\tau_{Z/E}$/ps	τ_T/ps
			Z-**1**			
CH	30.9	56 ± 12	$2 \times 10^{-2} \pm 2 \times 10^{-2}$	1.8	1.8	
THF	37.4	28 ± 6	$4 \times 10^{-1} \pm 4 \times 10^{-1}$	1.1	1.1	357
CH_2Cl_2	40.7	15 ± 3	$2 \times 10^{-1} \pm 2 \times 10^{-1}$	0.8	0.8	207
DMSO	45.1	1.8 ± 0.4	$2 \times 10^{-2} \pm 2 \times 10^{-2}$	0.6	0.6	13
			Z-**2**			
CH	30.9	44 ± 9	$2 \times 10^{-1} \pm 2 \times 10^{-1}$	17	17	
THF	37.4	2.5 ± 0.5		0.3	0.3	250
CH_2Cl_2	40.7	0.3 ± 0.1	$6 \times 10^{-3} \pm 6 \times 10^{-3}$	0.4	0.4	26
DMSO	45.1	0.2 ± 0.1	$2 \times 10^{-3} \pm 2 \times 10^{-3}$			7.0
			Z-**3**			
CH	30.9	30 ± 7	$3 \times 10^{-2} \pm 3 \times 10^{-2}$	6.1	6.1	75[a]
THF	37.4	17 ± 4	$3 \times 10^{-2} \pm 3 \times 10^{-2}$	2.8	2.8	75[a]
CH_2Cl_2	40.7	7.3 ± 1.7	$1 \times 10^{-1} \pm 1 \times 10^{-1}$	1.2		81
DMSO	45.1	1.5 ± 0.4	$3 \times 10^{-2} \pm 3 \times 10^{-2}$	1.8		54
			Z-**4**			
CH	30.9	32 ± 7	$1 \times 10^{-1} \pm 1 \times 10^{-1}$	4.8	4.8	
THF	37.4	29 ± 7	$1 \times 10^{-1} \pm 1 \times 10^{-1}$	12	12	
CH_2Cl_2	40.7	20 ± 5	$1 \times 10^{-1} \pm 1 \times 10^{-1}$	10	10	
DMSO	45.1	14 ± 3	$2 \times 10^{-1} \pm 2 \times 10^{-1}$	41	41	

[a]Values could not unambiguously be assigned.

polarity of the solvent. Therefore, T must be strongly polar, as one would expect for a state with significant charge-transfer character—similar to TICT states. The time constants τ_{SE} and τ_T vary considerably with solvent polarity for HTI *Z*-**1**. We found a steady decrease of τ_{SE} from 1.8 ps in CH to <0.2 ps in acetonitrile, while τ_T first increases with increasing solvent polarity to a maximum of 357 ps (THF) and then decreases again with increasing solvent polarity to 13 ps (acetonitrile or DMSO).

A similar analysis of the excited-state dynamics was performed for HTIs *Z*-**2** and *Z*-**3** (see Figure 4c,d, Figures S6 and S7, and Tables S6 and S7). The results are also summarized in Table 1. The behavior of *Z*-**2** matches that of HTI *Z*-**1** very closely and is analyzed in more detail in the Supporting Information. HTI *Z*-**2** undergoes efficient photoisomerization in unpolar CH, but in more-polar solvents a new excited state with spectral characteristics (ESA and SE) very similar to those of the state T of HTI *Z*-**1** is seen (Figure 4d). The state T in HTI *Z*-**2** is also strongly polar and decays faster with increasing solvent polarity (e.g., τ_T = 250 ps in THF and 7.0 ps in DMSO). HTI *Z*-**3** shows an overall similar behavior to *Z*-**1** and *Z*-**2**, but some differences are also observed. The 2D plot of the absorption changes (Figure S7) shows the appearance of a new state with increased ESA in the red spectral range. Within our spectral detection window, we observed no clear indication for stimulated emission, even at the longest wavelengths. Apparently ESA dominates in this region. As in HTI *Z*-**1**, the new state T of HTI *Z*-**3** grows in on the 1 ps time scale after the initial absorption transients and the formation of S_{1Min}. The T state is unambiguously identified for solvents with polarity larger than that of CH_2Cl_2. For less-polar solvents, indications for long-lasting absorption changes with very small amplitudes and somewhat different spectral signatures were found. A clear assignment to the excited state T was not possible in this case.

Time-Resolved Fluorescence. For a better understanding of the properties of the excited-state time-resolved emission, experiments have been performed for HTI *Z*-**1** in selected solvents (Figure 5a and Figures S9–S11). Time-resolved fluorescence of HTI *Z*-**1** in the medium-polar solvent CH_2Cl_2 is shown in Figure 5a. At time zero, an intense and rapidly decaying component can be seen in the spectral range from 520 to 600 nm. At longer wavelengths between 575 and 700 nm, a long-lasting emission is observed. A global fit function applied to the data revealed two time constants. The fast time constant of ~2.4 ps at shorter wavelength, being below the instrumental response function, gives only an upper limit for the lifetime of this fluorescent state. The long-lasting emission at longer wavelength decays with a time constant of 195 ps. The short- and the long-lived emitting states are assigned to S_{1Min} and T, respectively. An estimate of the total emission indicates that both components contribute to the stationary fluorescence emission. A more detailed analysis[55] of the emission using the small fluorescence quantum yield (2×10^{-1}%) of HTI *Z*-**1** can be found in the Supporting Information. It indicates that there is a considerable change of the transition dipole moment between S_{1Min} and the long-lived emitting state T, pointing to a strong change in the configuration of HTI *Z*-**1** in the excited electronic state.

Also in solvents with much higher polarity, two fluorescence components are detected in the time-resolved emission experiment. For example, in DMSO, a dominant signal with a maximum around 600 nm at time zero is found (Figure S11). From its rapid decay and spectral position, we could identify the short-lived state as S_{1Min}. The second component ranges from 600 to over 760 nm, with a maximum around 700 nm. The fluorescence data were again analyzed with a global fit function. The fast time constant was fitted with 1.4 ps and only represents an estimate of the lifetime of the corresponding

DOI: 10.1021/jacs.6b05981
J. Am. Chem. Soc. 2016, 138, 12219–12227

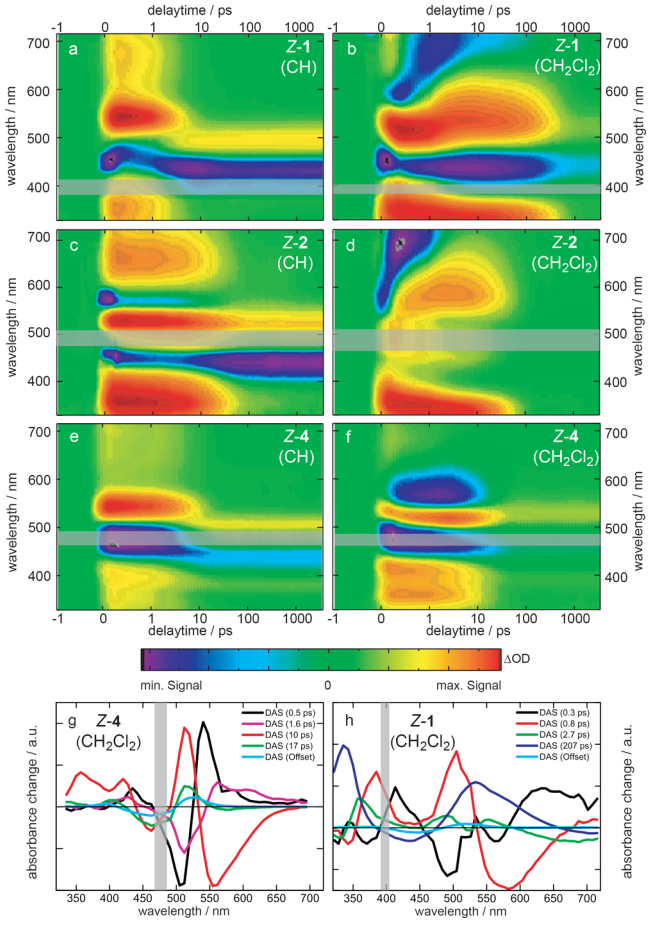

Figure 4. Transient absorption data for HTIs *Z*-**1**, *Z*-**2**, and *Z*-**4** in CH and CH_2Cl_2 as solvent. Gray transparent bars indicate missing data points due to scattering of the excitation wavelength. (a–f) Color-coded absorption difference plotted versus delay time and wavelength: (a), (c), and (e): *Z*-**1**, *Z*-**2**, and *Z*-**4** show similar behavior in CH. GSB and SE overlap at early delay times around 470 nm. SE and ESA decay on a time scale of few ps and a signal due to isomerization remains. (e) and (f): *Z*-**4** shows similar behavior in CH and CH_2Cl_2. SE is shifted to longer wavelengths and separated from the GSB in CH_2Cl_2. (b) and (d): *Z*-**1** and *Z*-**2** show similar ESA to *Z*-**4** in CH_2Cl_2 immediately after excitation. But within the first ps new features in the ESA appear and SE at shorter wavelength decays whereas a new strongly red-shifted SE appears. (g, h) The DAS of the global fit for *Z*-**1** and *Z*-**4** in CH_2Cl_2 are plotted versus wavelength: spectral characteristics of the decay of the initial populated states are drawn in red, those of state T in dark blue.

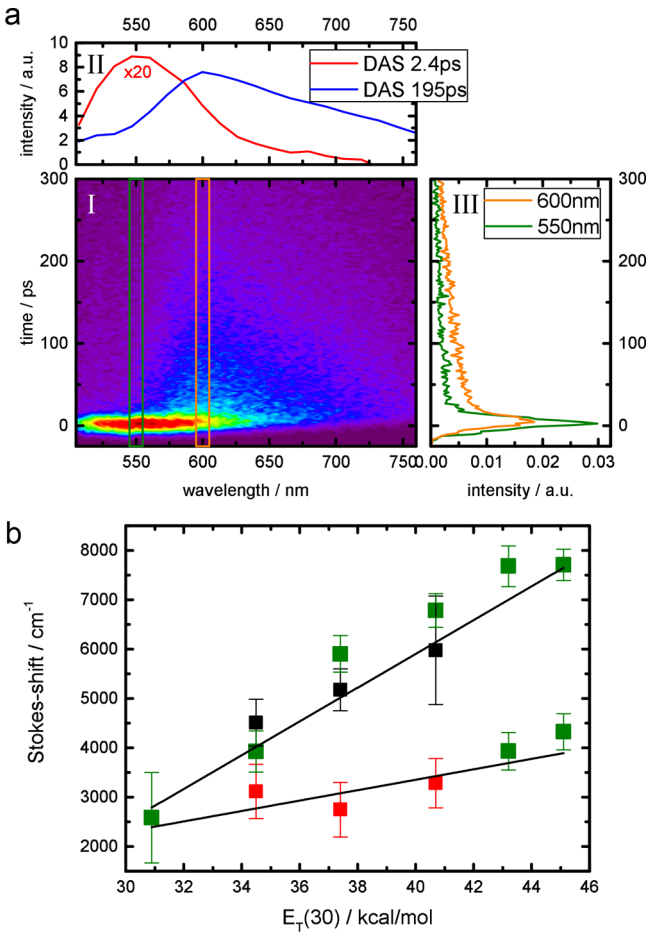

Figure 5. Fluorescence data of HTI *Z*-**1**. (a) Time-resolved fluorescence of *Z*-**1** in CH_2Cl_2. Inset I: Fluorescence intensity, plotted versus fluorescence wavelength and delay time. Inset II: The long-lasting component has a time constant of 195 ps. The DAS of the fast-decaying component is ca. 20 times larger than that of the slow-decaying component. Inset III: Time dependence of the fluorescence at the wavelengths 550 and 600 nm. (b) Stokes shift versus solvent polarity. Green squares show the Stokes shift taken from stationary measurements. In strongly polar solvents, two maxima due to dual fluorescence could be clearly separated. Red squares show the Stokes shifts of the fast-decaying component with a small dependence on solvent polarity. In contrast, the slow-decaying components (black squares) show a strong dependence on solvent polarity, indicating a highly polar state T.

excited state. As compared to the behavior of HTI *Z*-**1** in CH_2Cl_2, an even stronger change in dipole moment between the excited states S_{1Min} and T is found in more polar DMSO.

For the different solvents investigated, we always found the long decay times of the fluorescence emission in close vicinity to the respective lifetimes of the component T (τ_T) identified in the time-resolved absorption experiments. Apparently, emission and absorption experiments addressed the same state T. Its decay times τ_T strongly depend on solvent polarity (see Table 1).

The Stokes shifts of the two fluorescing components are displayed in Figure 5b versus solvent polarity (represented by the $E_T(30)$ values). As a general trend, one finds a weak red-shift of the rapidly decaying component with solvent polarity. This behavior is comparable to the solvatochromism of the fluorescence of *Z*-**4** (Figure 3). For the long-lasting component, the red-shift increases much more strongly. This pronounced solvent dependence of the long-lived fluorescence component points to a highly polar state T, whereas the short-lived state S_{1Min} should be less polar.

Quantum Yields. Quantum yields of the *Z*/*E* photoisomerization reaction ($\phi_{Z/E}$) of HTI *Z*-**1** to *Z*-**4** were measured in different solvents. The quantum yields $\phi_{Z/E}$ strongly depend on solvent polarity for HTI *Z*-**1** to HTI *Z*-**3** but considerably less so for HTI *Z*-**4**. The results are summarized in Table 1. HTIs *Z*-**1** to *Z*-**3** show a very strong decrease of $\phi_{Z/E}$ with increasing solvent polarity. A linear relationship between $\phi_{Z/E}$ and solvent polarity parameters is found for all solvents, as shown in Figure S3. In contrast, HTI *Z*-**4** shows only a small decrease of $\phi_{Z/E}$ with solvent polarity, which is also less linear. The measured fluorescence quantum yields are always very small.

DOI: 10.1021/jacs.6b05981
J. Am. Chem. Soc. 2016, 138, 12219–12227

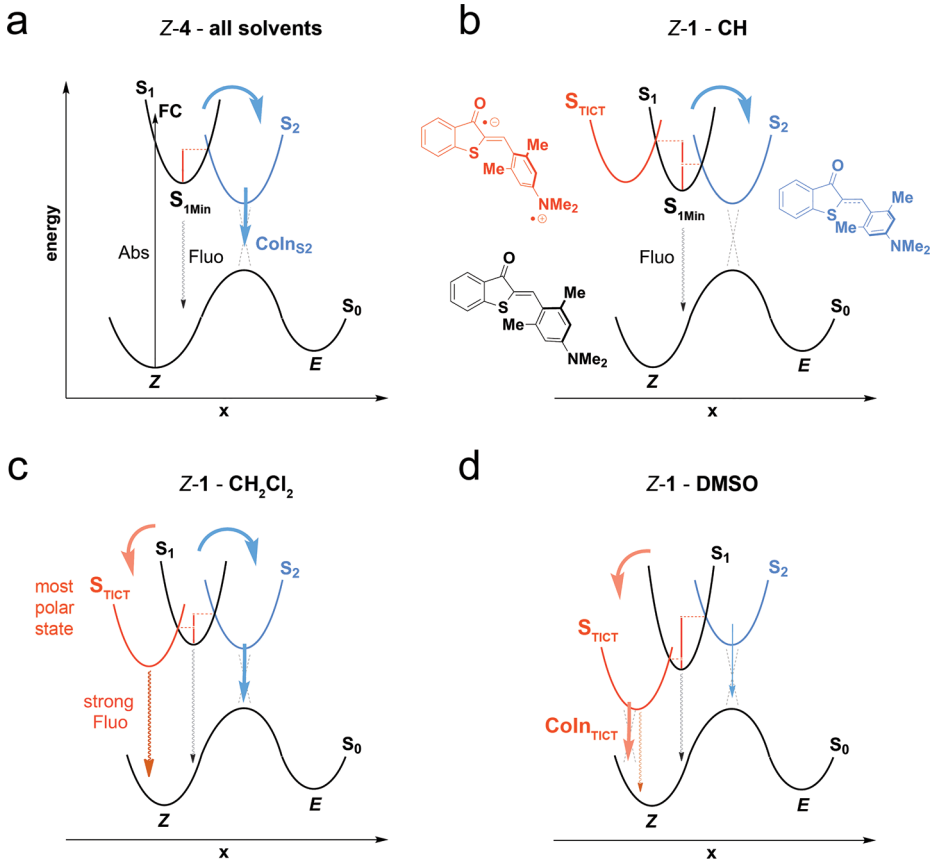

Figure 6. Model for the excited-state behavior of twisted HTIs exemplified for *Z*-**1** and *Z*-**4**. The different de-excitation pathways are indicated by bold colored arrows. Energy barriers are indicated by red bars. (a) For HTI *Z*-**4** the de-excitation proceeds via the photoisomerization of the double bond using a conical intersection ($CoIn_{S2}$) between the S_2 (blue potential well) and the S_0 states. To reach this $CoIn_{S2}$, the excited population has to leave the initially reached S_{1Min} state (black potential well) and cross a barrier when trespassing to the S_2 hyperpotential surface. (b) For HTI *Z*-**1**, a highly polar TICT state (red potential well) is not accessible in nonpolar solvents, and de-excitation proceeds from the S_{1Min} state via the double-bond isomerization pathway. Fluorescence (dotted arrow) is only observed from the S_{1Min} state. (c) In solvents of medium polarity, the TICT state is significantly stabilized and becomes populated. The energetically difficult direct transition from the TICT to the S_0 state leads to its slow de-excitation kinetics and therefore dominant stationary fluorescence from the S_{TICT}. (d) In solvents of very high polarity, TICT state stabilization leads to the opening of another radiationless de-excitation channel via rotation around the single bond. The rapid depopulation of the TICT state allows the fluorescence of the population in the S_{1Min} state to be seen as a second blue-shifted fluorescence band.

Viscosity Studies. The stationary fluorescence spectra of HTIs *Z*-**1** to *Z*-**3** were measured in solvents of different viscosity but similar polarity. Additionally, the presented time-resolved data can be analyzed in terms of viscosity influences. The data are shown and discussed in detail in the Supporting Information. From these studies it can be concluded that solvent viscosity is not responsible for the formation of state T, and its lifetime is not influenced significantly by viscosity either. On the other hand, there is a certain influence of viscosity on the S_{1Min} state and its decay. Since the S_{1Min} decay in polar solvents depends on both photoisomerization and TICT formation, viscosity influences cannot be attributed easily to either of these processes. In comparison to solvent polarity, the effects of viscosity on the de-excitation behavior of twisted HTIs are rather small.

DISCUSSION

The de-excitation and photoisomerization pathways of unsubstituted HTI have been described essentially as a motion along the double-bond isomerization coordinate, where a seam of conical intersections determines the transition to the electronic ground state.[29] A moderate positive solvatochromism of stationary absorption and fluorescence as well as a small dependence of the quantum yield $\phi_{Z/E}$ on solvent polarity should result from such a reaction. The quantum yield for the double-bond isomerization $\phi_{Z/E}$ does not even reach values around 50% since conical intersections close to the double-bond rotation coordinate lead back to the *Z* isomer prior to 90° rotation. This behavior is observed for all planar HTI photoswitches studied so far[31,36,37,56−58] and is supported by the theoretical description of unsubstituted HTI.[29] The planar compound HTI *Z*-**4** investigated here shows exactly this behavior (Figure 6a).

The ultrafast kinetics observed after photoexcitation of HTI *Z*-**1** show an odd solvent dependence with very severe changes of the de-excitation behavior. In unpolar CH, a canonical behavior is found with fast de-excitation and efficient photoisomerization. Apparently, a rotation of the central double bond is the dominant de-excitation pathway, despite pre-twisting around the single bond in the ground state. The latter may be the reason for the high quantum yield of HTI *Z*-**1** photoisomerization ($\phi_{Z/E}$ = 56%), the highest yet reported for this class of photoswitches. The kinetics measured for this process are considerably faster than for the corresponding photoisomerization of planar HTI *Z*-**4** ($\tau_{Z/E}$ = 1.8 ps for *Z*-**1**, $\tau_{Z/E}$ = 4.8 ps for *Z*-**4**). This behavior changes dramatically if

DOI: 10.1021/jacs.6b05981
J. Am. Chem. Soc. 2016, 138, 12219−12227

solvents with moderate or high polarity are used. Not only is there a change in the lifetime of the initially reached minimum of the excited electronic state S_{1Min}, but also a new long-lived and very polar state T is observed with long-wavelength ESA and fluorescence emission in the red and near-infrared. The lifetime of T is in the 100 ps range for solvents of moderate polarity and is shortened in solvents of very high polarity, e.g., τ_T = 22 ps in DMF or τ_T = 13 ps in DMSO and acetonitrile. In these solvents, the dominant de-excitation pathway is no longer *Z*/*E* photoisomerization, which results in very low quantum yields of double-bond isomerization, $\phi_{Z/E}$ < 5%.

Apparently, the de-excitation pathway of HTI *Z*-**1** can be changed by the choice of solvent. In nonpolar solvents such as CH, photoexcited *Z*-**1** photoisomerizes efficiently around the central double bond with high quantum yields and at very fast rates. The stationary absorption and fluorescence energies as well as excited-state spectral characteristics and kinetics are quite similar to the ones observed for the initially planar HTI *Z*-**4**. In solvents of intermediate polarity, a new excited state T with long lifetimes (up to 357 ps in THF) is formed, which is not seen in planar HTIs. At the same time, the photoisomerization quantum yield $\phi_{Z/E}$ decreases. If a very polar solvent is used, then the photoisomerization of *Z*-**1** is not efficient anymore, and de-excitation proceeds along a different coordinate with fast kinetics, leading to short excited-state lifetimes in the 20 ps time range. The fluorescence of the long-lived state T of HTI *Z*-**1** is strongly red-shifted in polar solvents, leading to very large Stokes shifts of more than 200 nm (Figure 5b), but its quantum yield ϕ_{fl} remains very low. Such strong effects of the solvent polarity on the fluorescence energy indicate a very polar excited state T having a different geometry than the ground state. In order to explain the observed solvent effects on the de-excitation of HTI *Z*-**1**, we refer to other photoisomerizing systems like donor−acceptor substituted stilbenes where the twist around a single bond leads to TICT states. The characteristics found for state T of HTI *Z*-**1** in polar solvents support the idea that T is indeed a state with pronounced TICT character (see Figure 6) and is hence called the TICT state in the following.[38,59] The TICT minimum on the S_1 hyperpotential surface is most likely characterized by severe twisting of the stilbene fragment around the C−C single-bond coordinate, which leads to efficient decoupling from the thioindigo fragment. This particular geometry is assumed because only derivatives *Z*-**1** to *Z*-**3**, which are pre-twisted along the C−C single-bond axis, form TICT states. Assuming TICT formation via the rotation of the dimethylamino group along the C−N single-bond axis would require additional conjugation breaking within the stilbene moiety and seems less likely. HTI *Z*-**2** possesses only one rotatable single bond, which connects the thioindigo with the stilbene fragment and serves as the TICT coordinate. The extremely similar behavior of *Z*-**1** and *Z*-**2** with respect to all quantified data gives additional strong evidence that the C−C single bond is indeed the axis of rotation for TICT formation in HTI *Z*-**1**. As a result of this twisting, charges can accumulate strongly on the two molecular fragments (negative charge on the thioindigo and positive charge on the stilbene fragment), leading to a highly polar species.

Depending on the solvent polarity, three different mechanistic scenarios have to be specified that involve the TICT state and are discussed exemplarily for *Z*-**1** in the following (see Figure 6). In nonpolar solvents such as CH, the TICT state is not accessible for HTI *Z*-**1**, as the solvent cannot stabilize this strongly polar state (Figure 6b). The energy of the TICT state remains high compared to that of the less polar S_{1Min} state, which is therefore exclusively populated from the FC region.[29,31] The stationary fluorescence observed for *Z*-**1** in CH can be fully attributed to the S_{1Min} state and is similar to the fluorescence seen for *Z*-**4** in the same solvent. From the S_{1Min} state, a barrier is crossed leading to the S_2 conical intersection $CoIn_{S2}$, and double-bond isomerization takes place. This finding remains to be true for *Z*-**1**, despite its sizable pre-twisting in the ground state, which typically facilitates TICT formation.[59−61] Thus, in CH *Z*-**1** does not rotate around the single bond but rather around the double bond during de-excitation, resulting in high quantum yields $\phi_{Z/E}$.

In solvents of intermediate polarity, such as CH_2Cl_2 or THF, the TICT state is strongly stabilized because it is the most polar state and becomes easily accessible for HTIs *Z*-**1** to *Z*-**3** (Figure 6c). From the initially populated S_{1Min}, two reaction pathways are available, rotation around the double bond coordinate with isomerization and rotation around the single bond toward the TICT state T with subsequent internal conversion (IC) to the initial *Z* isomeric ground state. For HTI *Z*-**4**, no indication for the population of the TICT state T is found in any solvent. Apparently, the planar geometry leads to a very high barrier on the way to the TICT state, which prohibits TICT formation. As the majority of TICT states for planar systems is described for strong donor and acceptor substituents,[40−45] it is likely that HTI *Z*-**4** lacks a sufficiently polarized double bond to enable single-bond rotation in the excited state. However, HTIs *Z*-**1** to *Z*-**3** have donor substitution very similar to that of HTI *Z*-**4** yet undergo TICT formation. For HTIs *Z*-**1** to *Z*-**3**, pre-twisting of the stilbene fragment in the ground state S_0 must lower the reaction barrier and facilitate TICT formation in the appropriate solvents. Formation of a TICT state leads to the typical prolonged radiative lifetimes, as the direct transition from the TICT state to the ground state is usually slow.[62] Due to inefficient IC to the initial ground state, long excited-state lifetimes τ_{TICT} are found for HTIs *Z*-**1** to *Z*-**3** in medium-polar solvents, and the stationary fluorescence is dominated by the TICT state. Despite TICT formation, sizable $\phi_{Z/E}$ values are still observed, which decrease with increasing solvent polarity.

Further increase in the solvent polarity leads to even stronger stabilization of the TICT state relative to the S_{1Min} state, which shifts a greater population of excited molecules into the TICT state with faster rates and therefore decreases the photoisomerization quantum yield $\phi_{Z/E}$ (Figure 6d). In this way the decrease of $\phi_{Z/E}$ with increasing solvent polarity can be explained. In very polar solvents like DMF or DMSO, *Z*/*E* photoisomerization is almost completely suppressed for HTI *Z*-**1**. Instead, a rapid de-excitation (13−22 ps) leads back to the *Z* conformation in the ground state, and two distinguished fluorescence bands are now clearly observed in the stationary spectra. The energy of the blue-shifted fluorescence is very similar to the fluorescence energy of HTI *Z*-**4** in the same (very polar) solvents, corresponding to the emission from the S_{1Min}. The strongly red-shifted fluorescence is a typical indication for a strongly polar S_{TICT} state. The overall behavior is consistent with formation of a TICT state that efficiently converts to the ground state via rotation of the single bond. The rapid radiationless de-excitation leads to a sizable decrease of the TICT state population and its fluorescence intensity, which now allows fluorescence of the shortly populated S_{1Min} state to be seen clearly together with the S_{TICT} fluorescence. In the proposed model, the strong stabilization of the TICT state in

DOI: 10.1021/jacs.6b05981
J. Am. Chem. Soc. 2016, 138, 12219−12227

very polar solvents brings it close to the S_0 hyper-potential energy surface. The proximity of the two states opens a new de-excitation channel via single-bond rotation, leading to significantly faster de-excitation of the TICT state. This channel is not well accessible for the less-stabilized TICT states in intermediate polar solvents, which explains the long τ_T lifetimes in, e.g., THF or CH_2Cl_2.

The behavior of HTI *Z*-**2** mirrors that of *Z*-**1** closely in every aspect, which strongly suggests the same C−C single-bond rotation as TICT coordinate in both compounds. The only significant difference is the apparent higher polarity of the TICT state in *Z*-**2**, leading to a much stronger response to solvent polarity. Therefore, the diminishing of $\phi_{Z/E}$ and TICT lifetime is already very pronounced in THF and CH_2Cl_2. This can easily be explained by the stronger donor character of the julolidine ($\sigma^+ = -2.03$) substitution in comparison to dimethylamine ($\sigma^+ = -1.70$).

One remaining question is the inter-dependence of photoisomerization and TICT formation. Are these two pathways mutually independent, and if so, when does the branching between pathways occur in polar solvents, where both processes contribute to the de-excitation? Mutual independence is strongly suggestive in CH versus DMSO based on the greatly different quantum yields for the photoisomerization. The time-dependent absorption data clearly show that the TICT state is populated on the same time scale as the decay of the SE representing the decay of the S_{1Min}. It seems likely that a sequential process takes place in which the S_{1Min} excited state is populated first, and the branching into double-bond isomerization or TICT formation occurs afterward from that state. Evidence for this mechanism is provided by the occurrence of a dominating, rapidly decaying, and slightly solvatochromic fluorescence as well as SE components possessing similar intensity regardless of the solvent used. Those fluorescence and SE characteristics were assigned to the S_{1Min} state also present in *Z*-**2**, *Z*-**3**, and *Z*-**4**. Their decay kinetics are affected by both double-bond isomerization and TICT formation and are therefore faster if both processes contribute, i.e., in solvents of medium and strong polarity.

For *Z*-**3**, a long-lived excited state with red-shifted spectral characteristics is already seen in the nonpolar CH solvent. However, the quantum yield of photoisomerization is still very high, with $\phi_{Z/E}$ = 30%. Also, the stationary fluorescence is not significantly shifted compared to those of *Z*-**1**, *Z*-**2**, and *Z*-**4** in the same solvent. In more polar solvents, the long-lived excited state becomes more dominant with increasing polarity. In contrast to the behavior of *Z*-**1** and *Z*-**2**, however, the lifetime of this excited state does not decrease significantly in very polar solvents like DMF or DMSO. The stationary fluorescence does not show any dual fluorescence in any solvent measured. For HTI *Z*-**3**, the ground-state twisting of the stilbene moiety is probably not as severe as in *Z*-**1** and *Z*-**2**, as is indicated by the crystallographic data. For this reason, it must be more difficult to reach a strongly twisted TICT state for this derivative. Therefore, TICT stabilization by solvent polarity might also be less effective for *Z*-**3**, precluding an efficient de-excitation pathway via single-bond rotation, even in very polar solvents. Whether the long-lived excited state observed in CH is also a TICT state—which would be counterintuitive given the high polarity of TICT states—or if instead an excited-state planarization takes place[63] will be clarified in future studies. The short N−S distance of 2.84 Å found in the crystal structure of *Z*-**3** would hint at a possibly positive interaction facilitating such planarization in apolar solvents.

CONCLUSION

In this work we have established an unprecedented control over the photoinduced intramolecular rotations of HTI photoswitches. The introduction of ground-state twisting of the stilbene moiety in combination with strong electron donor substitution allowed us to effectively choose the type of light-induced motion by simply changing the solvent polarity. For the most severely twisted HTI *Z*-**1**, the highest quantum yield for *Z*/*E* photoisomerization (around 50%) yet reported for this class of photoswitches was found in CH as solvent. This translates into 100% rotation along the double bond axis (at the conical intersection 50% of the molecules rotate back to the *Z* isomer, and only 50% proceed further to the *E* isomer). In DMSO this quantum yield drops dramatically to <5%, and the excited-state deactivation proceeds to more than 90% via single-bond rotation of the stilbene moiety to the initial ground state. We explain this behavior by a new mechanism involving the formation of a TICT state, which was characterized thoroughly using a variety of quantitative methods. Ultrafast absorption and fluorescence spectroscopy allowed us to follow the de-excitation directly and decipher the mechanism in great detail. In the future we will explore this exquisite control over the light-induced motions of HTI photoswitches in the context of molecular machines and sophisticated functional materials.

ASSOCIATED CONTENT

Supporting Information

The Supporting Information is available free of charge on the ACS Publications website at DOI: 10.1021/jacs.6b05981.

Detailed synthesis of HTIs *Z*-**1** to *Z*-**4** including full characterization, determination of physical properties including extinction coefficients, fluorescence and photoisomerization quantum yields, thermal stability of HTIs *E*-**1** to *E*-**4**, time-resolved absorption and fluorescence measurements in different solvents, conformational analysis in solution, stationary absorption, fluorescence, and excitation spectra in different solvents, ^1H and ^{13}C NMR spectra, and crystal structural data, including Schemes S1−S4, Figures S1−S50 and Tables S1−S10 (PDF)

X-ray crystallographic data for HTI *Z*-**2** (CIF)

X-ray crystallographic data for HTIs *Z*-**1**, *Z*-**3**, and *Z*-**4** (CIF)

AUTHOR INFORMATION

Corresponding Author

*heduch@cup.uni-muenchen.de

Author Contributions

§S.W. and B.M. contributed equally.

Notes

The authors declare no competing financial interest.

ACKNOWLEDGMENTS

H.D. thanks the "Fonds der Chemischen Industrie" for a Liebig fellowship and the Deutsche Forschungsgemeinschaft (DFG) for an Emmy-Noether fellowship. We further thank the DFG (SFB 749, A5 and A12) and the Clusters of Excellence 'Munich-Center for Advanced Photonics' and 'Center for

DOI: 10.1021/jacs.6b05981
J. Am. Chem. Soc. 2016, 138, 12219−12227

Integrated Protein Science Munich' (CIPS^{M}) for financial support.

REFERENCES

(1) Dal Molin, M.; Verolet, Q.; Soleimanpour, S.; Matile, S. *Chem. - Eur. J.* **2015**, *21*, 6012.
(2) Erbas-Cakmak, S.; Leigh, D. A.; McTernan, C. T.; Nussbaumer, A. L. *Chem. Rev.* **2015**, *115*, 10081.
(3) Kay, E. R.; Leigh, D. A.; Zerbetto, F. *Angew. Chem., Int. Ed.* **2007**, *46*, 72.
(4) Kelly, T. R.; De Silva, H.; Silva, R. A. *Nature* **1999**, *401*, 150.
(5) Hernandez, J. V.; Kay, E. R.; Leigh, D. A. *Science* **2004**, *306*, 1532.
(6) Koumura, N.; Zijlstra, R. W. J.; van Delden, R. A.; Feringa, B. L.; Harada, N. *Nature* **1999**, *401*, 152.
(7) Greb, L.; Lehn, J. M. *J. Am. Chem. Soc.* **2014**, *136*, 13114.
(8) Guentner, M.; Schildhauer, M.; Thumser, S.; Mayer, P.; Stephenson, D.; Mayer, P. J.; Dube, H. *Nat. Commun.* **2015**, *6*, 8406.
(9) Muraoka, T.; Kinbara, K.; Aida, T. *Nature* **2006**, *440*, 512.
(10) Haberhauer, G.; Kallweit, C.; Wölper, C.; Bläser, D. *Angew. Chem., Int. Ed.* **2013**, *52*, 7879.
(11) Ragazzon, G.; Baroncini, M.; Silvi, S.; Venturi, M.; Credi, A. *Nat. Nanotechnol.* **2015**, *10*, 70.
(12) Russew, M. M.; Hecht, S. *Adv. Mater.* **2010**, *22*, 3348.
(13) Göstl, R.; Senf, A.; Hecht, S. *Chem. Soc. Rev.* **2014**, *43*, 1982.
(14) Wang, X.; Huang, J.; Zhou, Y.; Yan, S.; Weng, X.; Wu, X.; Deng, M.; Zhou, X. *Angew. Chem., Int. Ed.* **2010**, *49*, 5305.
(15) Qu, D. H.; Wang, Q. C.; Zhang, Q. W.; Ma, X.; Tian, H. *Chem. Rev.* **2015**, *115*, 7543.
(16) Dube, H.; Rebek, J., Jr. *Angew. Chem., Int. Ed.* **2012**, *51*, 3207.
(17) Dube, H.; Ajami, D.; Rebek, J., Jr. *Angew. Chem., Int. Ed.* **2010**, *49*, 3192.
(18) Dube, H.; Ams, M. R.; Rebek, J., Jr. *J. Am. Chem. Soc.* **2010**, *132*, 9984.
(19) Venkataramani, S.; Jana, U.; Dommaschk, M.; Sonnichsen, F. D.; Tuczek, F.; Herges, R. *Science* **2011**, *331*, 445.
(20) Li, Q.; Fuks, G.; Moulin, E.; Maaloum, M.; Rawiso, M.; Kulic, I.; Foy, J. T.; Giuseppone, N. *Nat. Nanotechnol.* **2015**, *10*, 161.
(21) Yu, Z.; Hecht, S. *Angew. Chem., Int. Ed.* **2011**, *50*, 1640.
(22) Goldau, T.; Murayama, K.; Brieke, C.; Steinwand, S.; Mondal, P.; Biswas, M.; Burghardt, I.; Wachtveitl, J.; Asanuma, H.; Heckel, A. *Chem. - Eur. J.* **2015**, *21*, 2845.
(23) Broichhagen, J.; Podewin, T.; Meyer-Berg, H.; von Ohlen, Y.; Johnston, N. R.; Jones, B. J.; Bloom, S. R.; Rutter, G. A.; Hoffmann-Roder, A.; Hodson, D. J.; Trauner, D. *Angew. Chem., Int. Ed.* **2015**, *54*, 15565.
(24) Laprell, L.; Repak, E.; Franckevicius, V.; Hartrampf, F.; Terhag, J.; Hollmann, M.; Sumser, M.; Rebola, N.; DiGregorio, D. A.; Trauner, D. *Nat. Commun.* **2015**, *6*, 8076.
(25) Cahova, H.; Jäschke, A. *Angew. Chem., Int. Ed.* **2013**, *52*, 3186.
(26) Samanta, S.; Qin, C.; Lough, A. J.; Woolley, G. A. *Angew. Chem., Int. Ed.* **2012**, *51*, 6452.
(27) Kitzig, S.; Thilemann, M.; Cordes, T.; Rück-Braun, K. *ChemPhysChem* **2016**, *17*, 1252.
(28) Steinwand, S.; Halbritter, T.; Rastadter, D.; Ortiz-Sanchez, J. M.; Burghardt, I.; Heckel, A.; Wachtveitl, J. *Chem. - Eur. J.* **2015**, *21*, 15720.
(29) Nenov, A.; Cordes, T.; Herzog, T. T.; Zinth, W.; de Vivie-Riedle, R. *J. Phys. Chem. A* **2010**, *114*, 13016.
(30) Wiedbrauk, S.; Dube, H. *Tetrahedron Lett.* **2015**, *56*, 4266.
(31) Maerz, B.; Wiedbrauk, S.; Oesterling, S.; Samoylova, E.; Nenov, A.; Mayer, P.; de Vivie-Riedle, R.; Zinth, W.; Dube, H. *Chem. - Eur. J.* **2014**, *20*, 13984.
(32) Liu, R. S.; Asato, A. E. *Proc. Natl. Acad. Sci. U. S. A.* **1985**, *82*, 259.
(33) Liu, R. S.; Browne, D. T. *Acc. Chem. Res.* **1986**, *19*, 42.
(34) Müller, A. M.; Lochbrunner, S.; Schmid, W. E.; Fuß, W. *Angew. Chem., Int. Ed.* **1998**, *37*, 505.
(35) Saltiel, J.; Bremer, M. A.; Laohhasurayotin, S.; Krishna, T. S. *Angew. Chem., Int. Ed.* **2008**, *47*, 1237.
(36) Cordes, T.; Schadendorf, T.; Priewisch, B.; Rück-Braun, K.; Zinth, W. *J. Phys. Chem. A* **2008**, *112*, 581.
(37) Cordes, T.; Schadendorf, T.; Rück-Braun, K.; Zinth, W. *Chem. Phys. Lett.* **2008**, *455*, 197.
(38) Grabowski, Z. R.; Rotkiewicz, K.; Rettig, W. *Chem. Rev.* **2003**, *103*, 3899.
(39) Mukherjee, P.; Rafiq, S.; Sen, P. *J. Photochem. Photobiol., A* **2016**, *328*, 136.
(40) Karpicz, R.; Getautis, V.; Kazlauskas, K.; Juršėnas, S.; Gulbinas, V. *Chem. Phys.* **2008**, *351*, 147.
(41) Letard, J.-F.; Lapouyade, R.; Rettig, W. *J. Am. Chem. Soc.* **1993**, *115*, 2441.
(42) Pines, D.; Pines, E.; Rettig, W. *J. Phys. Chem. A* **2003**, *107*, 236.
(43) Rurack, K.; Dekhtyar, M. L.; Bricks, J. L.; Resch-Genger, U.; Rettig, W. *J. Phys. Chem. A* **1999**, *103*, 9626.
(44) Gruen, H.; Görner, H. *J. Phys. Chem.* **1989**, *93*, 7144.
(45) Singh, C.; Ghosh, R.; Mondal, J. A.; Palit, D. K. *J. Photochem. Photobiol., A* **2013**, *263*, 50.
(46) Yang, J.-S.; Lin, C.-J. *J. Photochem. Photobiol., A* **2015**, *312*, 107.
(47) Ernsting, N. P.; Breffke, J.; Vorobyev, D. Y.; Duncan, D. A.; Pfeffer, I. *Phys. Chem. Chem. Phys.* **2008**, *10*, 2043.
(48) Yang, S.; Han, K. *J. Phys. Chem. A* **2016**, *120*, 4961.
(49) Yang, J.-S.; Liau, K.-L.; Hwang, C.-Y.; Wang, C.-M. *J. Phys. Chem. A* **2006**, *110*, 8003.
(50) Yang, J.-S.; Liau, K.-L.; Wang, C.-M.; Hwang, C.-Y. *J. Am. Chem. Soc.* **2004**, *126*, 12325.
(51) Yang, J.-S.; Liau, K.-L.; Li, C.-Y.; Chen, M.-Y. *J. Am. Chem. Soc.* **2007**, *129*, 13183.
(52) Yamaguchi, T.; Seki, T.; Tamaki, T.; Ichimura, K. *Bull. Chem. Soc. Jpn.* **1992**, *65*, 649.
(53) Lougheed, T.; Borisenko, V.; Hennig, T.; Rück-Braun, K.; Woolley, G. A. *Org. Biomol. Chem.* **2004**, *2*, 2798.
(54) Eggers, K.; Fyles, T. M.; Montoya-Pelaez, P. J. *J. Org. Chem.* **2001**, *66*, 2966.
(55) Strickler, S. J.; Berg, R. A. *J. Chem. Phys.* **1962**, *37*, 814.
(56) Cordes, T.; Weinrich, D.; Kempa, S.; Riesselmann, K.; Herre, S.; Hoppmann, C.; Rück-Braun, K.; Zinth, W. *Chem. Phys. Lett.* **2006**, *428*, 167.
(57) Cordes, T.; Elsner, C.; Herzog, T. T.; Hoppmann, C.; Schadendorf, T.; Summerer, W.; Rück-Braun, K.; Zinth, W. *Chem. Phys.* **2009**, *358*, 103.
(58) Regner, N.; Herzog, T. T.; Haiser, K.; Hoppmann, C.; Beyermann, M.; Sauermann, J.; Engelhard, M.; Cordes, T.; Rück-Braun, K.; Zinth, W. *J. Phys. Chem. B* **2012**, *116*, 4181.
(59) Maus, M.; Rettig, W.; Bonafoux, D.; Lapouyade, R. *J. Phys. Chem. A* **1999**, *103*, 3388.
(60) Maus, M.; Rettig, W. *J. Phys. Chem. A* **2002**, *106*, 2104.
(61) Sasaki, S.; Niko, Y.; Klymchenko, A. S.; Konishi, G.-i. *Tetrahedron* **2014**, *70*, 7551.
(62) Van der Auweraer, M.; Grabowski, Z. R.; Rettig, W. *J. Phys. Chem.* **1991**, *95*, 2083.
(63) Verolet, Q.; Rosspeintner, A.; Soleimanpour, S.; Sakai, N.; Vauthey, E.; Matile, S. *J. Am. Chem. Soc.* **2015**, *137*, 15644.

DOI: 10.1021/jacs.6b05981
J. Am. Chem. Soc. 2016, 138, 12219−12227